Journal of Physics: Conference Series

PAPER • OPEN ACCESS

Exploring pressure effects on metallic nanoparticles and surrounding media through plasmonic sensing

To cite this article: C Martín-Sánchez *et al* 2020 *J. Phys.: Conf. Ser.* **1609** 012009

Exploring pressure effects on metallic nanoparticles and surrounding media through plasmonic sensing

C Martín-Sánchez[1], S Seibt[2], J A Barreda-Argüeso[1] and F Rodríguez[1*]

[1]Malta Consolider Team, DCITIMAC, Facultad de Ciencias, University of Cantabria, Av. de los Castros s/n, Santander 39005, Spain
[2] School of Engineering, RMIT University, Melbourne, Victoria 3004, Australia

rodriguf@unican.es

Abstract. The sensing capabilities of gold nanorods under high-pressure conditions were investigated in methanol-ethanol mixtures (up to 13 GPa) and in water (up to 9 GPa) through their optical extinction. The longitudinal SPR band of AuNR exhibits a redshift with pressure which is the result of two main competing effects: compression of the conduction electrons which increases the bulk plasma frequency (blueshift) and increase in the solvent density (redshift). The variation in de SPR peak wavelength allows us to estimate the bulk modulus of the gold nanoparticles with a precision of 10 % and to obtain analytical functions providing the pressure dependence of the refractive index of water in three phases: liquid, ice VI and ice VII. Furthermore, the SPR band shows abrupt jumps at the liquid to ice phase VI and ice phase VII transitions, which are in accordance with the first-order character of these transitions.

1. Introduction

The application of hydrostatic pressure to nanoscale materials is an efficient method to induce changes in their physico-chemical properties through volume reduction of both the nanoparticles and their surrounding medium. This is due to the ability of nanoscale materials to exhibit size dependent optical, magnetic, electronic and catalytic properties, which render them promising candidates for applications ranging from biomedicine to electronic displays [1-3]. However, a mayor challenge has been understanding and eventually predicting changes in nanomaterials properties due to structural changes of either the nanoparticles, the surrounding medium or both. This behavior can be monitored *via* surface plasmon resonances (SPR) in metal nanoparticles of various shapes (*e.g*. nanospheres and nanorods), due to changes in their aspect ratio (AR) or nanoparticle size, as well as in the refractive index of the surrounding medium.

The plasmonic properties of gold nanorod (AuNR) under high-pressure conditions have been recently exploited with such a purpose. This type of measurements allows us to probe the capability of AuNRs for nanosensing as pressure provides thoroughly changes of their optical properties. First pressure measurements have been done under severe nonhydrostatic conditions as nanoparticles were embedded in a matrix of ice [4] and phosphate glass [5], and later studies under quasihydrostatic regimes [6]. Nevertheless, few studies have been performed under hydrostatic conditions, enabling an adequate description of the SPR changes in terms of structural variations induced by pressure [7-9].

In this work we will show the suitability of AuNR to determine intrinsic properties of the nanoparticles as well as the pressure transmitting media (alcohol and water) by using the SPR spectral

shifts. This procedure enabled us to obtain information on the mechanical stiffness of the nano particles [8], or determine the variation of the refractive index $n(P)$ of the surrounding medium with pressure [9].

2. Experimental methods

2.1. Synthesis

Gold nanorods in MeOH-EtOH. AuNR dispersed in MeOH-EtOH solvents were prepared using hydroquinone as the reductant [10]. After rod growth, they were purified by centrifugation to remove CTAB and unreacted spectator ions. To stabilize the AuNR in the MeOH-EtOH solutions, a ligand exchange on the surfactant from CTAB to PVP (MW ≈ 10,000 g/mol) was carried out by stirring the AuNR samples in an excess PVP solution overnight and following purification by centrifugation with including solvent exchange. *Monodisperse gold nanorods in water*. First, standard AuNRs were synthesized via a seeded growth methot with minor modifications [11]. Then, the AR dispersity of the synthesized AuNRs was reduced via femtosecond pulsed laser treatment according to a previously published procedure [12].

2.2. Measurements

High-pressure experiments were carried out in a Boëhler-Almax diamond anvil cell (DACs). The 200 μm thick Inconel gaskets were preindented to 40-70 μm. The hydrostatic chamber consists of a 150 μm diameter holes perforated in the gasket with a BETSA motorized electrical discharge machine. The DAC was loaded with suitable MeOH-EtOH AuNR solutions and ruby microspheres (10-20 μm diameter) as pressure probes [13]. The solution itself acted as pressure-transmitting medium. In all experiments, the hydrostaticity of pressure-transmitting media was checked through the broadening of the ruby R-lines.

Optical absorption spectra under high-pressure conditions were collected on a home-built fiber-optic-based microscope [14], equipped with two Cassegrain 20× reflecting objectives mounted on two independent *x-y-z* translational stages, one for the microfocus beam, and another for the objective. A third independent *x-y* translation stage was used for positioning the DAC holder. Spectra in the ultraviolet-visible and near-infrared ranges were recorded with two spectrometers, an Ocean Optics USB 2000 and a NIRQUEST 512, employing Si- and InGaAs-CCD detectors, respectively. The I and I_0 transmitted intensities were measured in two separate experiments with the same DAC by loading it first with the nanoparticle solutions (I), and then with the corresponding solvent (I_0), covering the same pressure range. The hydrostatic pressure range and liquid-solid pressure transition of the AuNR solutions were determined from the pressure dependence of the full width at half maximum (fwhm) of the ruby R-lines.

3. Results and discussion

Figure 1 shows a representative transmission electron microscopy (TEM) image of AuNRs used in present measurements as well as their optical extinction spectra. The optical spectra show the characteristic band structure associated with the transversal SPR located at 510 nm (weak band) and the longitudinal SPR (strong band) at 740, 753 and 842 nm for solutions of AuNR with $AR = 3.4, 3.7$ and 4.9, respectively.

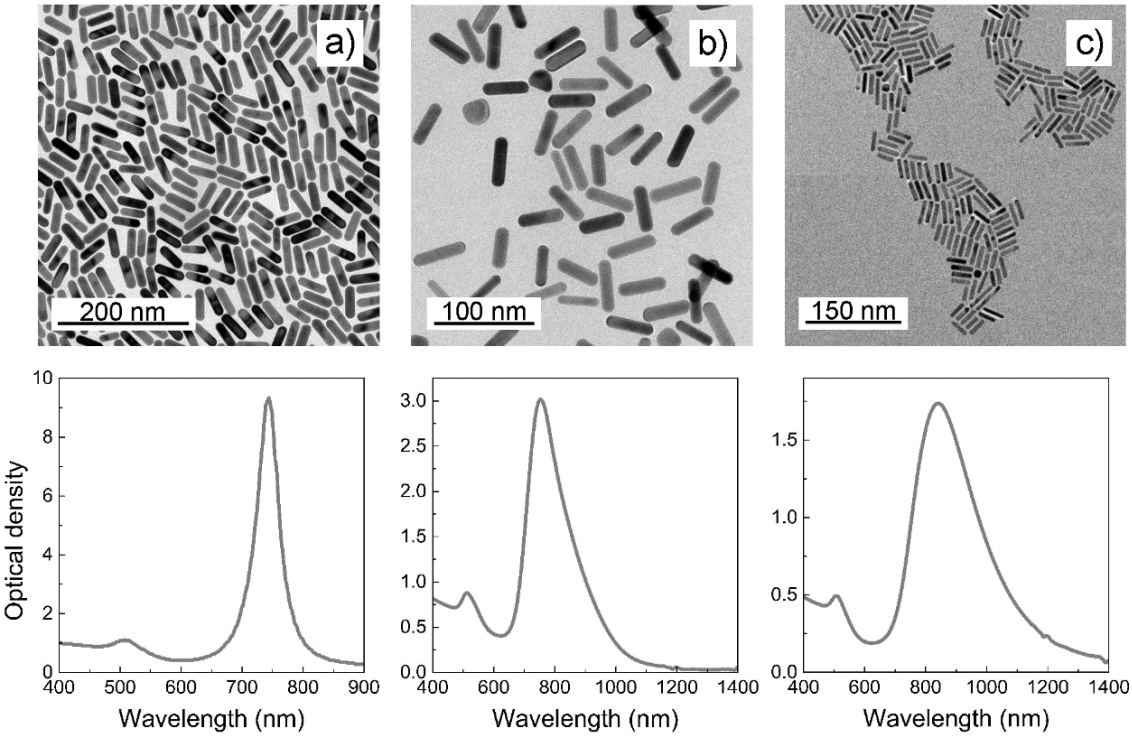

Figure 1. (Top) TEM images of the AuNRs used in pressure experiments. Particles resemble spherically capped cylinders with aspect ratios: a) $AR = 3.4$, b) $AR = 3.7$ and c) $AR = 4.9$. (Down) Optical extinction spectra of the corresponding AuNRs solutions dispersed in MeOH-EtOH with a volume ratio of 4:1.

The variation of the extinction spectra of AuNRs in MeOH-EtOH mixtures (4:1 and 1:4) with pressure shows a well-defined pressure-induced redshift of the LSPR for the AuNR solutions (figures 2 and 3). The LSPR shifts by about 9% of the LSPR wavelength from 0 to 10 GPa. Interestingly, the pressure induced redshift for the $AR = 4.9$ AuNR solution is 69 nm/GPa (0.12 eV/GPa) in the 0-0.5 GPa range, one of the largest pressure shifts recorded ever. It must be noted that Gans theory accounts fairly well for the pressure-induced LSPR shifts in the hydrostatic regime (liquid state), but it is inadequate for describing spectral variations after solidification of the pressure transmitting medium (non-hydrostatic conditions). The deviation of the measured optical extinction at the LSPR peak, $I(P)$, with respect to expectations of Gans theory is noteworthy (figure 2). As expected from model simulations, we observe an increase of $I(P)$ with pressure due mainly to an increase in the solvent refractive index under hydrostatic conditions. However, $I(P)$ shows an abrupt decrease with pressure at the solution solidification pressure. This behavior points out the inadequacy of Gans theory for describing the AuNR spectra under non-hydrostatic conditions. It is worth noting that whereas non-hydrostaticity of pressure transmitting media yields larger changes of $I(P)$ on solutions with a higher solidification pressure (P_{SOL} = 11 GPa in MeOH-EtOH 4:1), it occurs the opposite with the LSPR shift.

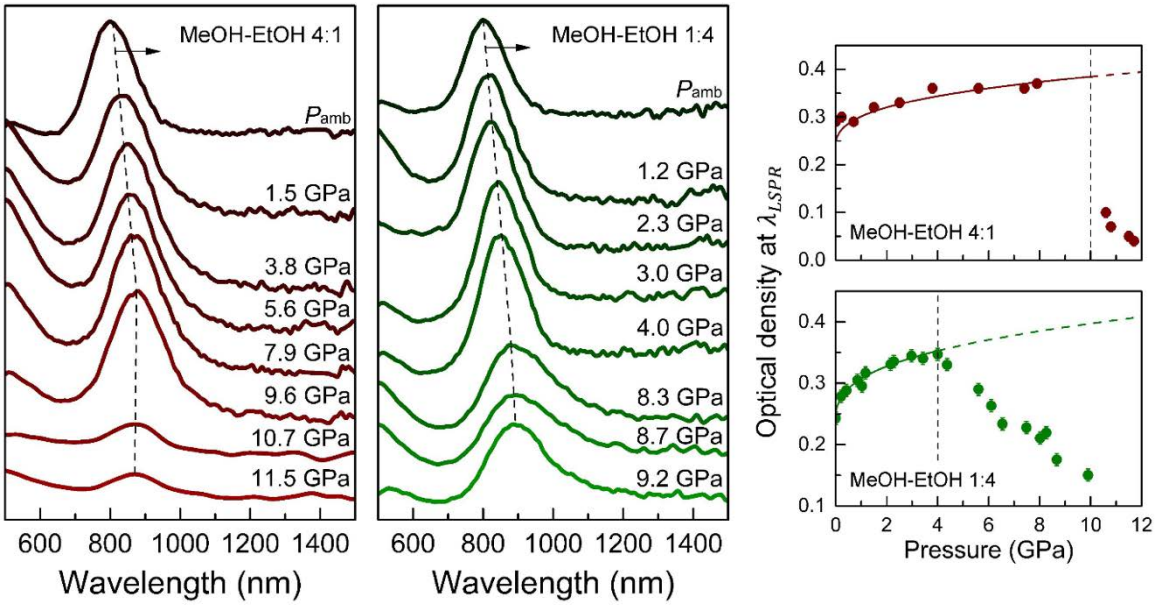

Figure 2. (Left) Spectra of $AR = 3.7$ AuNR in MeOH-EtOH 4:1 and (middle) 1:4 as a function of pressure. (Right) Plot of the optical density at the LSPR peak maximum versus pressure. Solid line: calculated extinction cross section from Gans theory for the two AuNR solutions. Dashed line: calculated cross section in the solidified solutions. Note the abrupt deviation of the experimental points at the solidification pressures: 4 and 10 GPa.

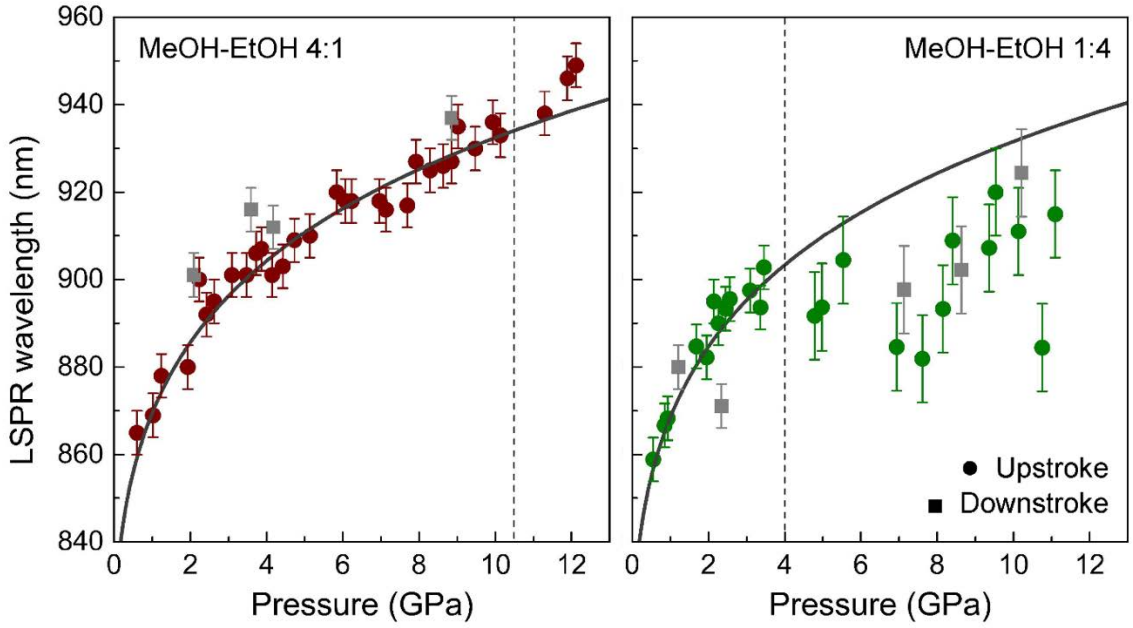

Figure 3. Pressure dependence of the LSPR peaks of $AR = 4.9$ AuNR solutions in MeOH-EtOH 4:1 and 1:4 (left and right plots, respectively). Plots include experimental and calculated values of $\lambda_{LSPR}(P)$ using the Gans model. This model accounts for the SPR behavior in the hydrostatic regime, but there are substantial deviations above the solidification pressure which is indicated with a vertical dashed line. Filled circles correspond to experimental data and lines represent the calculated LSPR wavelengths.

We analyze the variations of LSPR and associated extinction coefficient with pressure in terms of a Gans model [15] by considering the corresponding changes of the AuNR volume and solvent refractive index. The pressure dependence of the LSPR wavelength is obtained through the equation:

$$\lambda_{LSPR} = \lambda_p(0)\sqrt{\frac{V}{V_0}}\sqrt{\varepsilon(0) + \frac{1-L}{L}\varepsilon_m} \quad (1)$$

And the pressure dependence of the optical extinction at the LSPR peak through the equation:

$$I_{LSPR} = CV\varepsilon_m^{3/2}/\lambda_{LSPR} \quad (2)$$

Where $\lambda_p(0)$ and $\varepsilon(0)$ are the plasma wavelength at zero pressure and dielectric constant of gold at zero wavelength (infinite frequency), respectively. L is the AuNR depolarization or shape factor that was determined from the analysis of TEM images, $\varepsilon_m = n^2$ is the dielectric function of the non-absorbing medium (the pressure transmitting medium), V and V_0 are the molar volumes at zero-pressure and P, respectively, and C is a renormalization constant. To model the changes in the solvent refractive index with pressure, the dielectric function, $\varepsilon_m(P)$, is fitted empirically to a Lorentz-Lorentz relation

$$\varepsilon_m(P) = \frac{1+2u}{1-u} \quad (3)$$

where $u = \frac{4\pi}{3}\frac{N_A}{V_0}\left(\frac{V_0}{V}\right)\alpha_p$. Here N_A is the Avogadro's number and α_p is the molecular polarizability at P, that can be described empirically by the equation $\alpha_p = \alpha_0\left(\frac{V_0}{V}\right)^{\varphi}$ with $\varphi = -0.157$ for MeOH-EtOH 4:1 [16]. Using a Tait equation of state (EOS) for the solvent [17]

$$\frac{V_0}{V} = 1 - \frac{1}{(K_0'+1)}\ln\left[\frac{(K_0'+1)P}{K_0} + 1\right] \quad (4)$$

we obtain a precise description of the dielectric function of the solvent as a function of pressure by fitting the measured values to the equation

$$\varepsilon_m = \frac{1+2C_0\left(\frac{V_0}{V}\right)^{1+\varphi}}{1-C_0\left(\frac{V_0}{V}\right)^{1+\varphi}} \quad (5)$$

where C_0 and φ are determined by fitting the experimental $n(P)$ data to equation (5) and $V(P)$ data to equation (4) for the corresponding solvent. Using the available experimental refractive index and $V(P)$ data for liquid MeOH-EtOH 4:1 from 0 to 11 GPa [16], the obtained fitting parameters are $C_0 = 0.2109$, $K_0 = 0.77$ GPa and $K_0' = 9.9$. The change in the AuNR volume in this pressure range can be well described by a first-order Murnaghan EOS:

$$\frac{V}{V_0} = \left(\frac{PK_0'}{K_0} + 1\right)^{-1/K_0'} \quad (6)$$

Here K_0 and K_0' are the bulk modulus and its pressure derivative at zero pressure, respectively. Under hydrostatic load, we assume that the AuNR compresses isotropically (*fcc* crystal structure) thus keeping the AuNR *AR* constant with pressure. The λ_{LSPR} vs. P plot shown in figure 3 corresponds to the best fit to equation 1 obtaining a gold bulk modulus of $K_0 = 190$ GPa keeping fixed $K_0' = 6$ [8]. These results are consistent with x-ray diffraction measurements carried out on compacted Au nanospheres samples under nonhydrostatic conditions, the $V(P)$ of which can be described by an EOS with a bulk modulus of $K_0 = 196$ GPa [18], thus supporting our results under hydrostatic conditions. By contrast, a similar experiment [19] on concentrated Au nanosphere solutions revealed even more incompressible Au nanoparticles with $K_0 = 290$ GPa. Nanoparticle aggregation, sintering and

probably alloying effects, which are unavoidable when working with compacted nanoparticle samples, are likely responsible for these different results.

In order to exploit the sensing capabilities of AuNR in high pressure experiments, a series of experiments in aqueous AuNR solutions was performed to probe changes of the water refractive index. The idea is to explore an alternative method of measuring $n(P)$ in water, particularly, above the solidification pressure in ice phases. We have employed monodisperse AuNRs which were obtained by controlled irradiation with femtosecond laser pulses following a previously established procedure [12]. This method yields solutions with minimum dispersions in size and AR to increase the measurement accuracy to detect pressure-induced LSPR shifts. The usual AuNR solutions reported in the literature [20] have AR distributions with standard deviations of about 0.4, giving rise to LSPR bands with fwhm = 100 nm, and extinction coefficients at the LSPR maximum of 3000 nm^2. In contrast, monodisperse AuNR solutions have fwhm values of 50 nm and extinction coefficients of 8000 nm^2. From these values, we estimate that the signal-to-noise ratio of the extinction spectra of monodisperse AuNRs is improved by a factor 5.

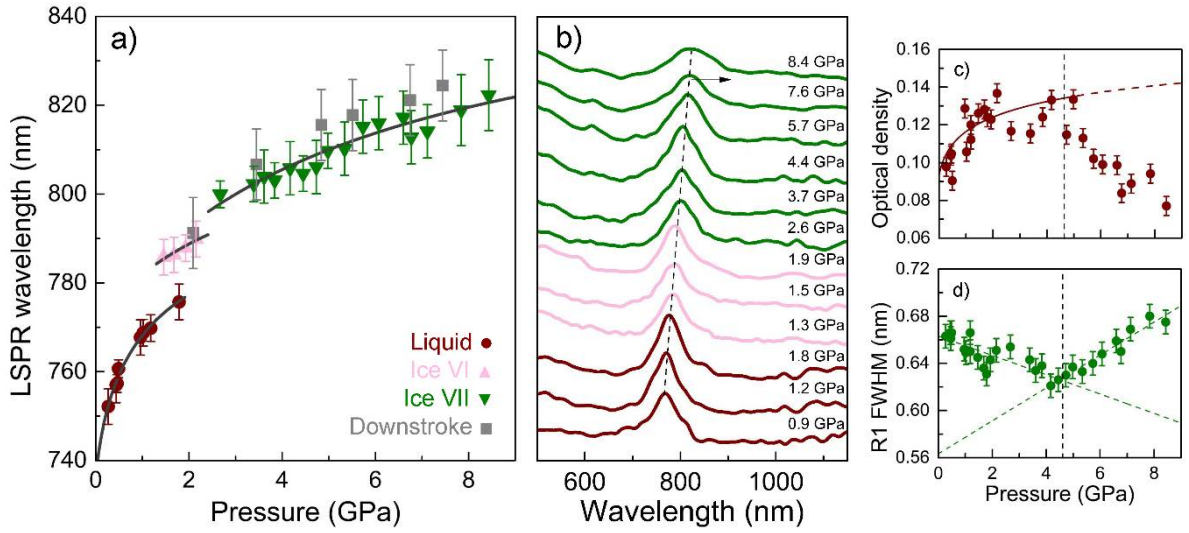

Figure 4. a) Pressure dependence of the LSPR peaks of $AR = 3.4$ AuNR solution in water. Filled circles correspond to experimental data and lines represent the calculated LSPR wavelengths. b) Extinction spectra of the solution as a function of pressure. c) Pressure dependence of the optical density at the LSPR band maximum. Solid line: calculated extinction cross-section from Gans theory. d) Hydrostatic pressure range of the solution. The vertical dotted line shows the hydrostatic limit of the pressure-transmitting medium. Note that after first solidification (liquid to ice VI transition at ~ 1.5 GPa) a quasi-hydrostatic regime is maintained.

The improved sensitivity allows us measuring optical spectra of more diluted solutions ([AuNR] = 3×10^{11} cm^{-3}) in DACs thus minimizing particle aggregation. Although high concentrated AuNR solutions improves the signal-to-noise ratio of the extinction spectra in DACs (light paths of about 70 μm), nanoparticle aggregation phenomena can yield additional spectral shifts [21] masking the intrinsic response of the individual AuNR.

Figure 4 shows the variation of the extinction spectra of aqueous AuNR solutions with pressure. A pressure-induced redshift of the LSPR is clearly observed in the explored pressure range. Furthermore, the LSPR redshift experiences abrupt jumps at each water phase, providing a spectroscopic way to identify phase-transition phenomena through plasmonics. The largest LSPR shift with pressure is measured in the low-pressure liquid phase and amounts to 22 nm/GPa (48 meV/GPa) around zero

pressure. In addition, LSPR jumps toward longer wavelengths at about 1.8 and 2.0 GPa, associated with the liquid to ice VI, and ice VI to ice VII phase transitions of water, respectively. We observe an increase in the optical density with pressure followed by an abrupt fall after hydrostaticity loss. Despite solidifying at low pressure, water displays a quasi-hydrostatic regime from 0 to 5 GPa. It is worth noting that, above this pressure, nonhydrostatic effects manifest themselves through a decrease of the optical density but barely affects the magnitude of LSPR pressure shifts.

As it was recently shown [9], LSPR spectral shifts of diluted AuNR aqueous solutions can be used to infer the value of $n(P)$ of the pressure transmitting medium, i.e. the solution. Particularly, the analysis of pressure-induced LSPR shifts on the basis of the Gans theory provides reliable $n(P)$ values in the liquid state as well as in the ice phases VI and VII (figure 5). We obtain $n(P)$ by fitting the experimental LSPR shifts to equation 1 using a phenomenological Murnaghan-type equation as:

$$n = n_0 \left(\frac{P\alpha}{\beta} + 1\right)^{1/\alpha} \tag{7}$$

where n_0 is the refractive index of water at ambient pressure, and α and β are fitting parameters. This procedure provides a semiempirical analytical function for defining $n(P)$ data for different phases of water: liquid, ice VI and ice VII (Table 1). This method is advantageous since it provides a more direct measure of refractive index in high-pressure experiments than other techniques such as Brillouin scattering [22] or interferometric techniques [23-25]. These techniques involve accurate measurements of two independent variables: the Brillouin peak shift and sound velocity, and the interference pattern and interlayer distance, respectively. Our surface-plasmon-based method depends on two main contributions: the solvent refractive index and the bulk modulus of gold in the nanoparticles. These two contributions are well known and can be easily decoupled, particularly for gold nanoparticles, because the contribution from electron gas compression accounts for <10% of the total contribution to the SPR pressure shifts.

Table 1. Fitting parameters to the Murnaghan-type equation for each investigated water phase. Pressure range of applicability is also included.

	Liquid	Ice VI	Ice VII
n_0	1.33 ± 0.01	1.40 ± 0.01	1.43 ± 0.03
α	26 ± 3	34 ± 3	13.7 ± 0.4
β	6 (fixed)	14 (fixed)	30 (fixed)
Pressure range (GPa)	0-1.8	1.5-2.2	2.2-9

The suitability of equation 7 to describe $n(P)$ of water was evaluated by comparison with experimental data reported by Polian *et al*. [22] and by Dewaele *et al*. [23], Vedam and Limsuwan [24] and Zha *et al*. [25] as it is shown in figure 5. We obtain similar $n(P)$ values for the liquid and ice VI phase as those reported in the literature [22-25]. In the more dispersed $n(P)$ of ice VII we find a better agreement with the results from ref [23] and [25], especially in the high pressure region (P > 5 GPa).

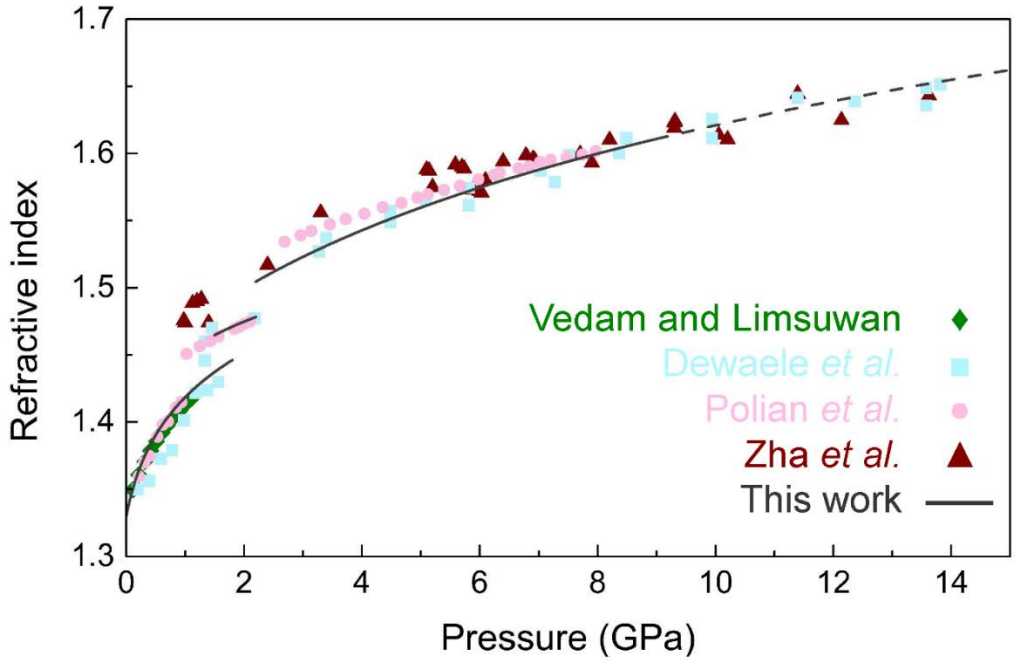

Figure 5. Pressure dependence of the refractive index of water. Filled points correspond to previous data: (diamond) Vedam and Limsuwan [24], (square) Dewaele *et al*. [23], (circles) Polian *et al*. [22] and (triangles) Zha *et al*. [25]. The later points were extracted from reported data by Zha *et al*. [25] and Pan *et al*. [26]. The solid lines represent experimental refractive index values obtained in this work. Dashed line is an extrapolation of our model outside the studied pressure range.

4. Conclusions

We have demonstrated that AuNRs dispersions have good sensing capabilities to explore physical properties of both the AuNR and solvent under high-pressure conditions. Pressure-induce changes in the AuNR LSPR can be accurately measured in DACs using monodisperse AuNR dispersions. Dilution prevents from nanoparticle aggregation thus enabling the study of independent AuNR particles and of the surrounding medium. The LSPR shift provides direct information on $n(P)$ and is an excellent sensor to detect structural phase transformations. First, we show that the bulk modulus of the AuNR increases by about 10% with respect to bulk gold, and, second, MeOH-EtOH AuNR solutions exhibit one of the largest pressure-induced LSPR redshift at low-pressure: 69 nm/GPa. Third we conclude that the AuNR solutions solidified at slightly different pressure with respect to pure solvent. Finally, Gans theory fairly accounts for the pressure-induced SPR shifts and variations of extinction cross section in the hydrostatic range. However, it can be inadequate for describing the AuNR spectral behaviour under nonhydrostatic conditions after solvent solidifications.

Acknowlegements

Financial support from Project PGC2018-101464-B-I00 (FEDER) and MALTA-Consolider Team (RED2018-102612-T) of the Ministerio de Ciencia, Innovación y Universidades is acknowledged.

References

[1] El-Sayed M A 2004 *Acc*. *Chem*. *Res*. **37** 326-333
[2] Pérez-Juste J, Pastoriza-Santos I, Liz-Marzán L M and Mulvaney P 2005 *Coord*. *Chem*. *Rev*.

249 1870-1901
[3] Nie S, Xing Y, Kim G J and Simons J W 2007 *Annu*. *Rev*. *Biomed*. *Eng*. **9** 257-288
[4] Bao Y, Zhao B, Tang X, Hoy D, Cai J, Tang S, Liu J, Wang F and Cui T 2015 *Appl*. *Phys*. *Lett*. **107** 201909
[5] Christofilos D, Assimpoulos S, Del Fatti N, Voisin C, Vallèe F, Kourouklis G A and Ves S 2003 *High Pressure Res*. **23** 23-27
[6] Gu W X, Hanson L A, Eisler C N, Koc M A and Alivisatos A P 2018 *Phys*. *Rev*. *Lett*. **121** 056102
[7] Medeghini F, Hettich M, Rouxel R, Silva Santos S D, Hermelin S, Pertreux E, Torres Dias A, Legrand F, Maioli P, Crut A, Vallée F, San Miguel A and Del Fatti N 2018 *ACS Nano* **12** 10310-10316
[8] Martín-Sánchez C, Barreda-Argüeso J A, Seibt S, Mulvaney P and Rodriguez F 2019 *ACS Nano* **13** 498-504
[9] Martín-Sánchez C, González-Rubio G, Mulvaney P, Guerrero-Martínez A, Liz-Marzán L M and Rodríguez F 2019 *J*. *Phys*. *Chem*. *Lett*. **10** 1587-1593
[10] Vigderman L and Zubarev E R 2013 *Chem*. *Mater*. **25** 1450-1457
[11] Scarabelli L, Grzelczak M and Liz-Marzán L M 2013 *Chem*. *Mater*. **25** 4232-4238
[12] González-Rubio G, Díaz-Núñez P, Rivera A, Prada A, Tardajos G, González-Izquierdo J, Bañares L, Llombart P, Macdowell L G, Alcolea-Palafox M, Liz-Marzán L M, Peña-Rodríguez O and Guerrero- Martínez A 2017 *Science* **358** 640-644
[13] Syassen K 2008 *High Pressure Res*. **28** 75-126
[14] Barreda-Argüeso J A and Rodríguez F Patent 2005 No. WO2015052356A1
[15] Gans R 1912 *Ann*. *Phys*. **342** 881-900
[16] Eggert J H, Su L W, Che R Z, Chen L C and Wang J F 1992 *J*. *Appl*. *Phys*. **72** 2453
[17] Tait P 1911 *Phys*. *Chem*. **2** 1
[18] Hong X, Duffy T S, Ehm L and Weidner D J 2015 *J*. *Phys*.*: Condens*. *Matter* **27** 485303
[19] Gu Q F, Krauss G, Steurer W, Gramm F and Cervellino A 2008 *Phys*. *Rev*. *Lett*. **100** 045502
[20] Link S, Mohamed M B and El-Sayed M A 1999 *J*. *Phys*. *Chem*. *B* **103** 3073-3077
[21] Nie Z, Fava D, Rubinstein M and Kumacheva E 2008 *J*. *Am*. *Chem*. *Soc*, **130** 3683-3689
[22] Polian A and Grimsditch M 1983 *Phys*. *Rev*. *B: Condens*. *Matter Mater*. *Phys* **27** 6409-6412
[23] Dewaele A, Eggert H J, Loubeyre P and Le Toullec R 2003 *Phys*. *Rev*. *B: Condens*. *Matter Mater*. *Phys* **67** 0094122
[24] Vedam K and Limsuwan P 1978 *J*. *Chem*. *Phys*. **69** 4772-4778
[25] Zha C, Hemley R J, Gramsch S A, Mao H and Bassett W A 2007 *J*. *Chem*. *Phys*. **126** 074506
[26] Pan D, Wan Q and Galli G 2014 *Nat*. *Commun*. **5** 3919